Hyperbolic Property of Earthquake Networks

Karla Henricksen* and Ilya Zaliapin†‡

September 30, 2019

Abstract

We examine the geometry of earthquakes in time-space-magnitude domain using the Gromov hyperbolic property of metric spaces. Gromov δ-hyperbolicity quantifies the curvature of a metric space via *four point condition*, which is a computationally convenient analog of the famous *slim triangle* property. We estimate the δ-hyperbolicity for the observed earthquakes in Southern California during 1981–2017. A set of earthquakes is represented by a point field in space-time-magnitude domain D. The separation between earthquakes is quantified by the Baiesi-Paczuski proximity η that has been shown efficient in applied cluster analyses of natural and human-induced seismicity and acoustic emission experiments. The Gromov δ is estimated in the earthquake space (D, η) and in the proximity graphs $\mathcal{G}_{\eta_0}$ obtained by connecting pairs of earthquakes within proximity η_0. All experiments result in the values of δ that are bounded from above and do not tend to increase as the examined region expands. This suggests that the earthquake field has hyperbolic geometry. We discuss the properties naturally associated with hyperbolicity in terms of the examined earthquake field. The results improve the understanding of the dynamics of seismicity and further expand the list of natural processes characterized by underlying hyperbolic geometry.

Key Words: Large scale geometry, Gromov δ-hyperbolicity, earthquake networks.

1. Introduction

Large scale geometry, which studies objects and spaces as if viewed from afar, is a well established area of mathematics, with specific ramifications in random walk theory, differential geometry, geometric topology, and more [26, 32]. During the recent decades large scale geometry has been recognized as an efficient tool for applied analysis of complex networks [23, 24]. In particular, the graphs that describe such diverse phenomena as the Internet, biological, social, or science networks, have shown to have *hyperbolic geometry* at large scale [7, 11, 17, 21, 22, 23]. This means that these graphs can be naturally embedded in spaces of negative curvature, as opposed to the familiar flat Euclidean space. *Krioukov et al.* [24] have shown that such common properties of observed complex networks as power law degree distribution and high cluster coefficient follow naturally from hyperbolicity of the embedding space. Moreover, the converse is also true – if a network has a power law degree distribution, then its underlying geometry is effectively hyperbolic. The underlying hyperbolicity has multiple tangible implications for structure and dynamics of networks. For instance, the self-similarity (a.k.a. scale-free property) of a network may reflect particular invariances of a hyperbolic space with respect to symmetry transformations [24]. Optimal routing (sending a message between two points in a shortest time)

*Department of Mathematics and Statistics, University of Nevada, Reno, NV, 89557

†Department of Mathematics and Statistics, University of Nevada, Reno, NV, 89557

‡This research is supported by NSF award EAR-1723033.

has a natural implementation in a hyperbolic network, avoiding the intrinsic complications that make this problem unsolvalbe in general graphs. This novel understanding explains an interest to applied analysis of observed networks, with the goal of revealing their underlying geometry [7, 11, 12, 17, 21, 22, 23, 24]. Here we perform a large scale geometric analysis of earthquakes in time-space-energy domain.

Seismicity is a complex natural phenomenon that poses important challenges for science and society [5]. Quantification of seismicity patterns is needed to mitigate the devastating economic and humanitarian impact of natural and human-induced earthquakes. The need for such research is highlighted by increasing population density in large urban areas near major active faults (e.g., Tokyo, Istanbul, Los Angeles, San Francisco), the catastrophic earthquakes in Japan, Haiti and Indonesia (life loss over 500,000, economical damage over $US 100 billion), and recent earthquakes in the Midwestern US and other areas with hydrocarbon and geothermal production [16].

Graph-theoretic analyses have shown efficient for better understanding the dynamics of seismicity on the intermediate time scales, from days to hundreds of years [1, 2, 4, 14, 27, 30, 31, 33, 34]. In this work, we estimate the large scale geometry of earthquakes proximity graphs, and the general earthquake proximity space, using Gromov δ-hyperbolicity that measures large scale curvature in a metric space. We find that the examined earthquake space and graphs exhibit strong δ-hyperbolicity. This sheds some light at space-time organization of seismicity and further expands the list of natural processes characterized by underlying hyperbolic geometry.

The rest of the paper is organized as follows. We begin by reviewing key facts about hyperbolic metric spaces in Sect. 2. In particular, we introduce Gromov δ-hyperbolicity via the Slim Triangle Condition and the Four Point Condition in Sect. 2.1. Section 3 discusses the proposed estimation approach and illustrates it in the Euclidean and hyperbolic planes. The earthquake data and necessary phenomenological background is described in Sect. 4. The Baiesi-Paczuski earthquake proximity that is used to measure separation between earthquakes in space-time-energy domain is described in Sect. 4.3. The main results are presented in Sect. 5 that performs hyperbolicity analysis in the proximity space of earthquakes, and in earthquake proximity graphs (combinatorial and metric). Section 6 concludes.

2. Background: Hyperbolic Metric Spaces

This section reviews the key concepts related to the hyperbolic metric spaces. Recall that a *metric* on a set X is a positive-definite symmetric function $d : X \times X \to [0, \infty)$ that satisfies the triangle inequality [9]. A pair (X, d), where X is a set and d is a metric on it, is called a *metric space*. A *geodesic* is the shortest path between two points in a metric space [9]. A metric space is called *geodesic* if any two points are connected by a geodesic path. The familiar n-dimensional Euclidean space $\mathbb{R}^n$ that consists of all points $\mathbf{x} = (x_1, \ldots, x_n)$ with Euclidean metric

$$d(\mathbf{x}, \mathbf{y}) = \sqrt{(x_1 - y_1)^2 + \cdots + (x_n - y_n)^2}$$

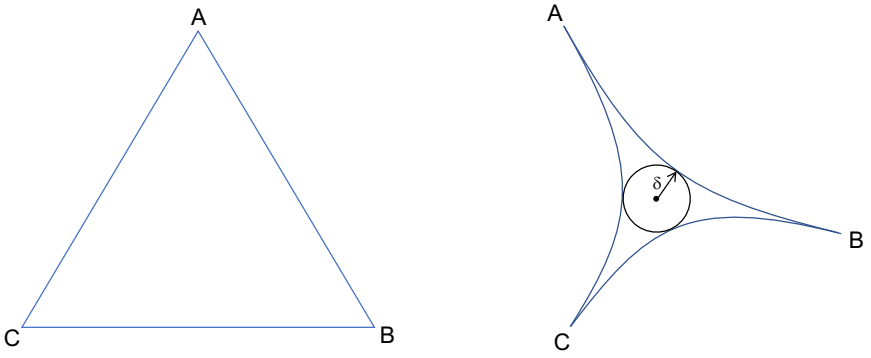

(a) Euclidean triangle (b) Hyperbolic (thin) triangle

Figure 1: Euclidean (a) and hyperbolic (b) triangles ABC.

is a geodesic metric space. The Euclidean metric plays a special role in the Euclidean space since this is the only metric (up to scaling) that is related to the inner product

$$d^2(\mathbf{x}, \mathbf{y}) = \langle \mathbf{x} - \mathbf{y}, \mathbf{x} - \mathbf{y} \rangle = \sum_i (x_i - y_i)^2.$$

The metric space $(\mathbb{R}^3, d)$ describes many familiar properties of the physical three-dimensional world around us. For instance, the geodesics are straight lines, the sum of the angles of any triangle equals π, the area of a circle growth polynomially with its radius r, as πr^2, and so on. Interestingly, many of these properties are tightly connected to the underlying *flat* geometry of the Euclidean space, which has been axiomatically described by Euclid via his five postulates [10]. One of them (parallel postulate) can be phrased in the following form: *Given a line and a point not on it, there is exactly one line going through the given point that is parallel to the given line.* An interesting alternative geometry arises when the parallel postulate is dropped, while the other four still hold. Some consequences of this omission are that geodesic lines are no longer straight but curved, the sum of angles in a triangle is not equal to π, and so on, resulting in curved spaces [10]. It can be shown that in an isotropic space, the parallel postulate can be violated in exactly two ways: there might be no parallel lines through a given point, which leads to so-called *spherical* (positively curved) geometry, or there exists an infinite number of parallel lines, which leads to *hyperbolic* (negatively curved) geometry [8, 10].

We are interested here in negatively curved *hyperbolic* spaces. An isotropic hyperbolic space is characterized by its constant *curvature* $K = -\zeta^2$ for some $\zeta > 0$. The hyperbolic triangles become *thin*, with the sum of the angles being less than π (and equal to zero for so-called *ideal* triangles); see Fig. 1. The area $A_\zeta(r)$ of a hyperbolic circle grows much faster than in Euclidean case, depending exponentially on the radius r [6]:

$$A_\zeta(r) = \frac{2\pi}{\zeta^2}(\cosh \zeta r - 1) = \frac{2\pi}{\zeta^2}\left(\frac{e^{\zeta r} + e^{-\zeta r}}{2} - 1\right) \sim \frac{\pi}{\zeta^2} e^{\zeta r} \quad \text{as } r \to \infty.$$

The two-dimensional hyperbolic distance $d = d(u, v)$ between points with polar coordinates

$u = (r_1, \theta_1)$ and $v = (r_2, \theta_2)$ is defined via the hyperbolic law of cosines [24]:

$$\cosh \zeta d = \cosh \zeta r_1 \cosh \zeta r_2 - \sinh \zeta r_1 \sinh \zeta r_2 \cos \Delta\theta, \tag{1}$$

where $\Delta\theta = \pi - \mid \pi - \mid \theta_1 - \theta_2 \mid\mid$ is the angle between u and v. It is straightforward to check that the above expressions for $A_\zeta(r)$ and d converge to the familiar Euclidean formulas as $\zeta \to 0$, i.e. when the space flattens.

The thin triangle property and exponential growth of circle area are closely connected to another informal statement: *a hyperbolic space is similar to a tree.* To develop intuition, consider a combinatorial tree with branching index b (so that all internal vertices have degree $b + 1$). In such a tree, the number of vertices at distance less or equal to r from a given one growth as b^r [24]. This is similar to how the area $A_\zeta(r)$ of a circle with radius r grows in a hyperbolic space with curvature $K = -(\ln b)^2$, i.e. with $\zeta = \ln b$. Furthermore, any triangle formed by three vertices in a tree is a tripod, which is the ultimate form of a thin triangle.

This tree analogy is made formal by various rigorous results that show how a hyperbolic metric can be approximated by a tree. For instance, consider a hyperbolic space X and any natural n. It can be shown that there exists such $C > 0$ that any n-element subset of X can be mapped to the set of leaves of a finite tree so that all distances are distorted by no more than C [9, Lemma 8.4.15].

The hyperbolic geometry of a space can be more complicated than that in a space of constant negative curvature. The degree of negative curvature of a space *at large scale* can be evaluated using the Gromov δ-hyperbolicity conditions discussed in the next section.

2.1 Slim Triangle and Four Point Conditions

Gromov δ-hyperbolicity is a measure of negative curvature in a metric space. There exist two main approaches to measuring δ-hyperbolicity. The first approach is based on the slim triangle condition, also known as the Rips condition.

Definition 1 (Slim Triangle Condition, [21])**.** *Consider a geodesic metric space (X, d). A triangle ABC with endpoints A, B, $C \in X$ is called δ-slim if there exists $\delta > 0$ such that any side of the triangle ABC is within δ of the union of the other two sides. Equivalently, the inscribed circle in the triangle has radius of no more than δ (Fig. 1b). A metric space in which all possible triangles are δ-slim is said to be δ-hyperbolic.*

This definition of δ-hyperbolicity is quite intuitive; however, it requires one to construct the *geodesics* between points which can be difficult to do in practice. A computationally convenient alternative is the *four point condition* that only requires the pairwise distances between points.

Definition 2 (Four Point Condition, [22])**.** *Given any four points A, B, C, and D, in a metric space (X, d) denote:*

$$L := d(A, B) + d(C, D), \tag{2}$$

$$M := d(A, C) + d(B, D), \tag{3}$$

$$S := d(A, D) + d(B, C), \tag{4}$$

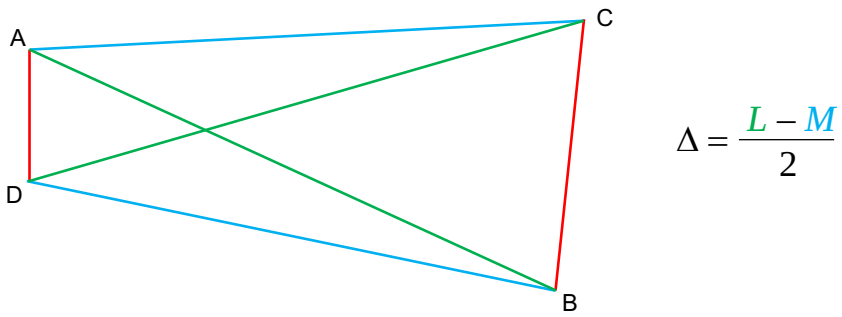

Figure 2: Four point condition: an illustration. Quadruple A, B, C, and D connected by geodesics, with corresponding diameter L (green), M (blue), and S (red).

such that $L \geq M \geq S$, relabeling if necessary (Fig. 2). Then the points A, B, C, D satisfy the δ-Four Point Condition for $\delta > 0$ if

$$\Delta := \frac{L - M}{2} \leq \delta. \tag{5}$$

We say a metric space satisfies the δ-Four Point Condition and is δ-hyperbolic if all possible quadruples satisfy the δ-four point condition.

The two definitions of δ-hyperbolicity are equivalent, differing only by a constant, as described by the next theorem.

Theorem 1 (Equivalence of the Slim Triangle and Four Point Conditions, [8])**.** *Suppose a metric space (X, d) is δ-hyperbolic according to the slim triangle condition. Then (X, d) satisfies the 2δ four point condition. Conversely, suppose (X, d) satisfies the δ four point condition. Then (X, d) is at most 6δ-hyperbolic according to the slim triangle condition.*

2.2 An upper bound on Δ

The following result gives an upper limit to the value of Δ for any given quadruple of points.

Theorem 2 (Upper bound for δ)**.** *Let A, B, C, and D be any four points in a metric space X. Then,*

$$\Delta = \frac{L - M}{2} \leq \min\{d(A, B), d(C, D)\}. \tag{6}$$

Proof. By definition,

$$\begin{aligned} \frac{L - M}{2} &= \frac{d(A, D) + d(B, C) - d(A, C) - d(B, D))}{2} \\ &= \frac{(d(A, D) - d(A, C)) + (d(B, C) - d(B, D))}{2} \\ &= \frac{(d(A, D) - d(B, D)) + (d(B, C) - d(A, C))}{2}. \end{aligned} \tag{7}$$

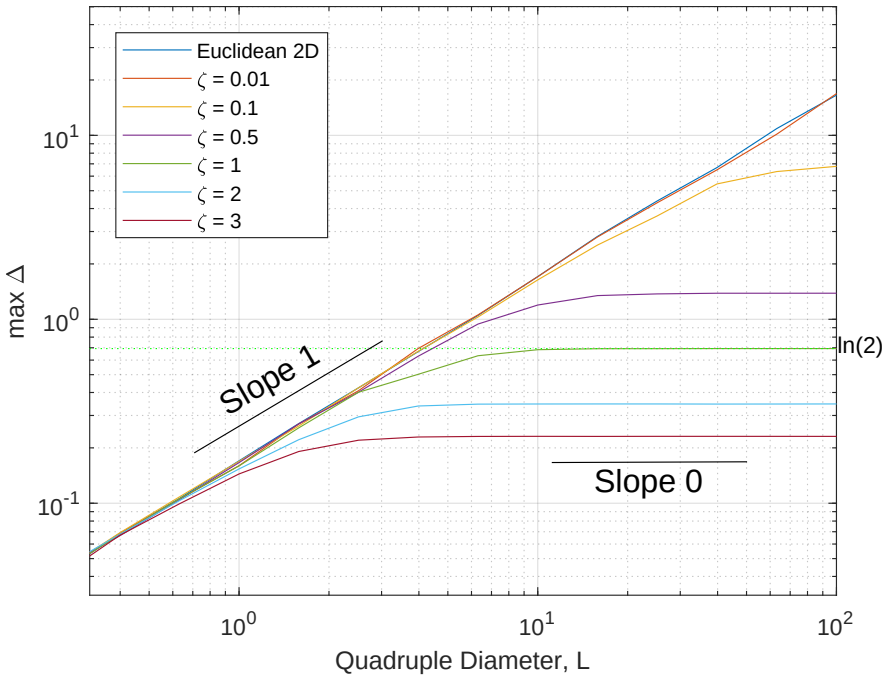

Figure 3: Gromov δ-hyperbolicity in a 2D space of constant curvature $K = -\zeta^2$. The value of $\max\{\Delta\} = \max\{(L-M)/2\}$ as a function of quadruple diameter L. In a (flat) Euclidean plane with $\zeta = 0$, $\max\{\Delta\} \propto L$ (blue line), which implies that there is no upper bound for Δ. In hyperbolic planes with $\zeta > 0$, $\max\{\Delta\}$ saturates as L increases. The existence of the maximal value implies δ-hyperbolicity. For instance, the hyperbolic plane with $\zeta = 1$ is δ-hyperbolic with $\delta = \ln 2$ (green horizontal line) in accordance with [25]. The experiment uses 100,000 uniform random quadruples for each plane.

The triangle inequality gives:

$$d(A,D) - d(A,C) \le d(C,D),$$

$$d(B,C) - d(B,D) \le d(C,D),$$

$$d(A,D) - d(B,D) \le d(A,B),$$

$$d(B,C) - d(A,C) \le d(A,B).$$

This immediately implies

$$\frac{L-M}{2} \le \min\{d(A,B), d(C,D)\},$$

which completes the proof. □

3. Estimating δ-hyperbolicity: An illustration

This section illustrates estimation of Gromov δ-hyperbolicity in Euclidean and hyperbolic spaces of constant curvature. In order to do this, we generate multiple quadruples of points that are uniformly distributed in a circle of radius R in either Euclidean plane or hyperbolic plane with constant curvature $K = -\zeta^2$. The δ-hyperbolicity is then estimated as

$$\delta = \max_i \{\Delta_i = (L_i - M_i)/2\},$$

where the maximum is taken over all simulated quadruples indexed by i. We also look at the behavior of $\Delta = (L - M)/2$ as a function of various parameters of the experiment, to establish the key qualitative patterns that distinguish flat from negatively curved space. This exercise highlights some essential properties of δ-hyperbolicity and ensures that, in a situation with a known answer, our statistical approach leads to correct estimation of the Gromov δ parameter.

Recall that the flat Euclidean plane corresponds to $\delta = \infty$, an isotropic hyperbolic plane with $\zeta > 0$ corresponds to a finite δ, and, in particular, $\zeta = 1$ corresponds to $\delta = \ln 2$ [25].

Our first experiment examines the behavior of $\Delta = (L - M)/2$ as a function of the quadruple diameter L. For that, we generate 1,000 quadruples in a circle of radius R, with 100 distinct values of R varying between $R = 10^{-3}$ and $R = 10^2$ on a logarithmic scale (hence producing 100,000 quadruples). Then we calculate Δ and L for each quadruple and plot the maximal value of $\Delta(L)$ vs. L (using some binning for L). Appendix A discusses how to generate uniform points in a hyperbolic circle. The results are shown in Fig. 3. In a flat Euclidean plane, Δ increases linearly with slope 1 as a function of the diameter L, in accordance with a straightforward analytic analysis. In a hyperbolic space, δ saturates and becomes a ζ-dependent constant as L increases, hence reflecting the curved geometry of the examined space. As the curvature (and parameter ζ) decreases, the saturation onset shifts to larger values of L, while for smaller values of L the curves get closer to the straight line of slope 1. This tells us that these spaces are essentially becoming "flatter" as ζ decreases. Lastly, we see that all curves are overlapping for small values of L, which means that when the quadruple points are very close to each other, the effect of negative curvature is practically unnoticeable. In other words, a sufficiently small neighborhood always has geometry of a flat (Euclidean) space.

Our second experiment examines the behavior of Δ as a function of radius R; see Fig. 4. For that, we generate multiple uniform quadruples in two-dimensional Euclidean space and two-dimensional hyperbolic space with constant curvature $\zeta = 1$, within circles of changing radius. First, we observe that in both flat and curved spaces, there is a positive monotone relation between R and L. This reflects the intuitive fact that large quadruples only may appear within circles of large radius. Furthermore, for small values of radius ($R \leq 1$) the flat and curved spaces behave similarly, confirming our earlier observation that small neighborhoods always have flat geometry. However, for larger radii ($R \geq 5$) the values of maximal Δ saturate with L in hyperbolic space, and keep linearly growing in Euclidean space. This is consistent with our earlier observation that curved hyperbolic geometry is best felt at large scales.

The results of this section suggest a useful benchmark – behavior of Δ as a function of L – against which one can assess the results for spaces with unknown geometry. This is what we do in the next sections.

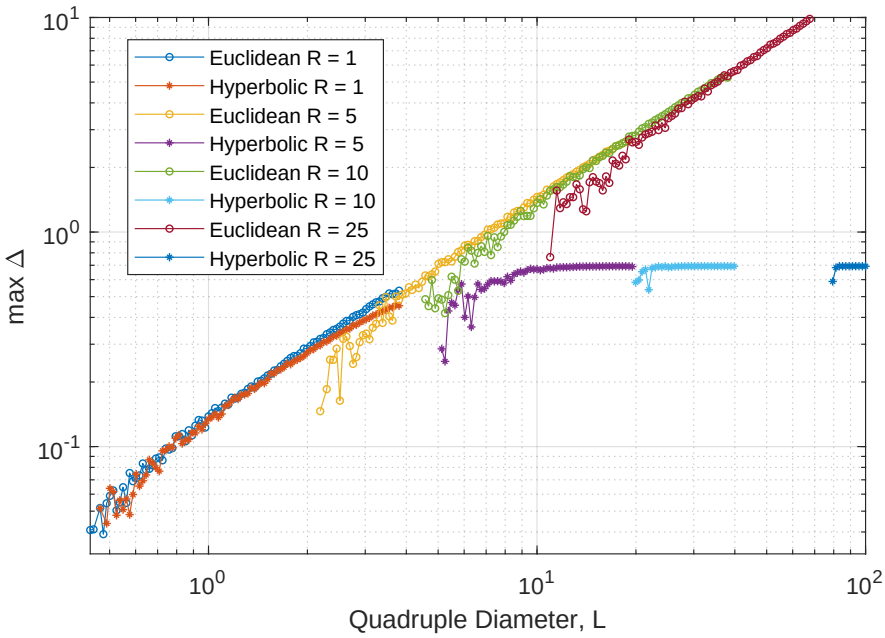

Figure 4: Δ in Euclidean plane (circles) and hyperbolic plane (stars) with $\zeta = 1$. Results for uniform quadruples within circles of different radii R. The experiment uses 50,000 uniform random quadruples for each value of R in each space.

4. Earthquakes: Data, proximity, and networks

This section describes the earthquake catalog examined in this study, introduces the space-time-magnitude earthquake proximity, which is the main tool of our metric analysis, and defines the earthquake proximity networks.

4.1 Data

In this study we examine geometry of earthquakes in Southern California. We work with the relocated catalog of *Hauksson et al.* [20] extended for the period 1981–2017. The catalog is available via the SCEC Data Center[1]. We focus primarily on the San Jacinto Fault Zone, the most active fault zone of the examined region. The same qualitative results are obtained for other subregions of Southern California and other seismically active regions. The examined catalog contains 18,972 earthquakes with magnitudes ranging from 1.50 to 5.43. For each registered earthquake i, the catalog reports its occurrence time t_i; location comprised of latitude λ_i, longitude ϕ_i, and depth z_i; and magnitude (a logarithmic measure of energy) m_i. The map of the examined catalog is shown in Fig. 5. The time-latitude projection of the examined earthquakes is shown in Fig. 6.

[1] `http://www.data.scec.org/research-tools/downloads.html`

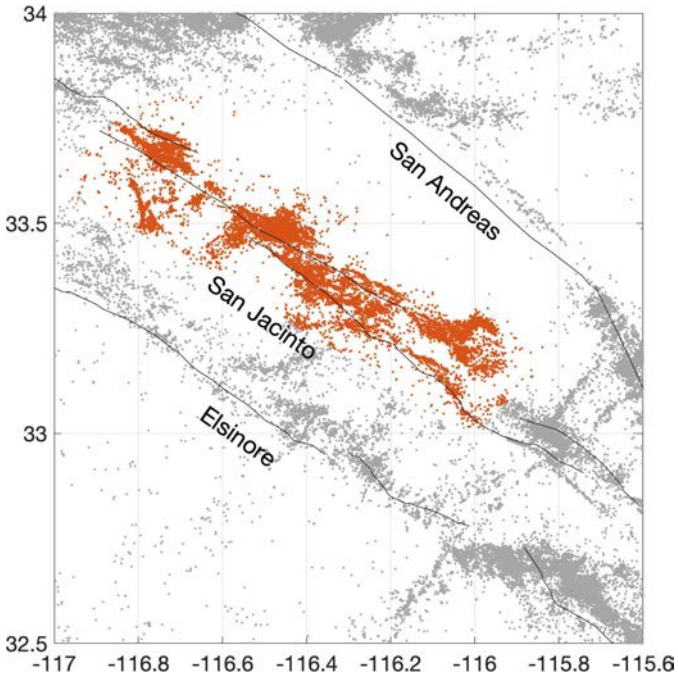

Figure 5: The study area in Southern California. Gray dots show the epicenters of earthquakes with magnitude $m \geq 1.5$ from the catalog of *Hauksson et al.* [20] extended to 2017. The red dots show the examined earthquakes within the San Jacinto Fault Zone. Black lines show the major faults.

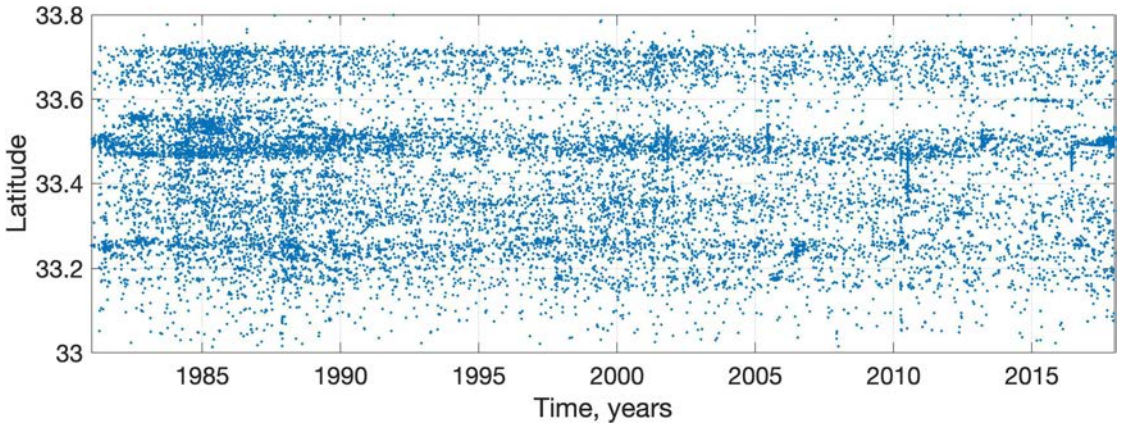

Figure 6: The time-latitude plot of the examined earthquakes.

4.2 Gutenberg-Richter law

The main empirical observation regarding earthquakes is the Gutenberg-Richter law, which states that the number N of earthquakes with magnitude above m is approximated by

$$\log_{10} N \approx a - bm, \tag{8}$$

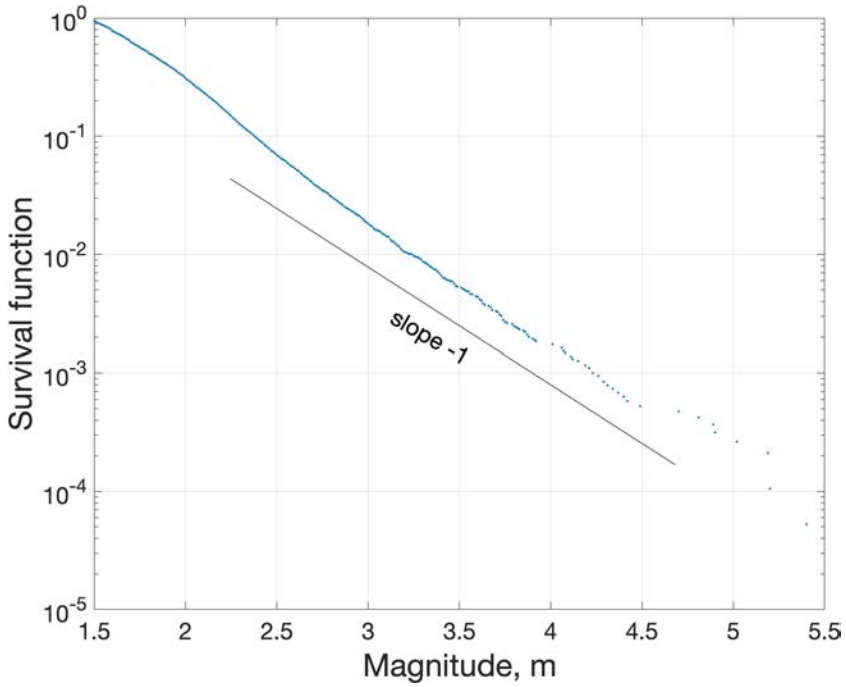

Figure 7: Empirical survival function $P(\text{magnitude} > m)$ for the examined earthquakes.

where $m \geq m_0$ and $b \approx 1$. The observed earthquakes closely follow this relation in different geographic regions and time ranges, although the first principles behind the law remain unsettled. Another empirical observation is that the magnitudes of consecutive earthquakes seem to be statistically independent.

One can interpret these observations via a statistical statement that the magnitude m of an earthquake, given $m \geq m_0$, follows an exponential distribution with parameter $\lambda = b \log_{10} e$. To see this, we rewrite the Gutenberg-Richter law as

$$P(\text{magnitude} \geq m) = 10^{a-bm}.$$

For the minimum magnitude $m = m_0$ this gives $10^{a-bm_0} = 1$, which implies $a = bm_0$. Accordingly,

$$P(\text{magnitude} \geq m) = 10^{bm_0-bm} = 10^{-b(m-m_0)} = e^{-b(m-m_0)\ln 10},$$

which we recognize as the survival function of an exponential distribution with parameter $\lambda = b \ln 10$. The empirical survival function for the examined earthquakes is shown in Fig. 7. A line that corresponds to the exponential tail decay with parameter $b = 1$, $\lambda = \ln 10$ is shown in the figure for visual comparison. One can see that the tail of the empirical distribution ($m > 2.5$) can be fairly closely approximated by the exponential distribution with $\lambda = \ln 10$. The observed deviations, in particular those seen for $m < 2.5$ are typical for the natural seismicity.

4.3 Baiesi-Paczuski proximity

An asymmetric proximity η_{ij} between an earthquake j and an earlier earthquake i is defined using the approach of *Baiesi and Paczuski* [4]:

$$\eta_{ij} = \begin{cases} t_{ij}(r_{ij})^d 10^{-bm_i}, & t_{ij} > 0, \\ \infty, & t_{ij} \leq 0, \end{cases} \tag{9}$$

where $t_{ij} = t_j - t_i$ is the time difference in seconds between the examined events, r_{ij} is the spatial distance in meters between the earthquake epicenters, d is the dimension of the epicenters, and $b \approx 1$ is the parameter of the Gutenberg-Richter law. In this work we use $d = 2$ and $b = 1$; accordingly, the proximity has units of [m^2·sec].

Note that this proximity is not a metric (distance) since it can be equal to zero for non-identical earthquakes (when $t_{ij} = 0$ or $r_{ij} = 0$) and it does not satisfy the triangle inequality (e.g., one always can connect any two points by two segments such that the points within the first have the same time coordinate, and the points within the second have the same spatial coordinate, resulting in zero length of the two segments). We notice that these deviations from the proper distance are solely due to the existence of distinct points with the same space or time coordinates. Roughly speaking, the proximity behaves as an asymmetric distance for large time and space separations between events, and hence can be considered as an approximation to a proper (unknown) metric in the time-space-magnitude domain of earthquakes.

An intuitive interpretation of the proximity is given in terms of a stationary homogeneous point process with exponential magnitudes and independent time, space, and magnitude components. Specifically, the proximity η_{ij} between points i and j equals the expected number of events in this process within the space-time cylinder between points i and j (i.e., the cylinder with the time projection $[t_i, t_j]$ and space projection being the circle centered at event j and with radius r_{ij}). Indeed, this is exactly how the Euclidean distance can be defined via a homogeneous point process with unit intensity. For a comprehensive discussion of the proximity, we refer to [33, 36].

The proximity η has shown instrumental in various analyses of seismicity, including scale-free properties of earthquake networks [4], earthquake cluster identification and classification with respect to the physical properties of the lithosphere [34, 35, 37], discriminating between natural and human-induced seismicity [28, 37], analysis of earthquake aftershocks and foreshocks [35, 19, 13, 18], and understanding triggering processes in rock fracture [15].

In this work, we assume that the minimal time separation between events is 1sec and the minimal space separation is 1m. This means that if two events occurred at a smaller separation, we artificially make it 1s and/or 1m; such cases are, however, very rare. We then use a logarithmic version of the proximity

$$\log_{10} \eta_{ij} = \log_{10} t_{ij} + d \log_{10} r_{ij} - b(m_i - m_{\max}) \geq 0$$

to quantify space-time-magnitude separation between pairs of earthquakes. All metric characteristics of the earthquake quadruples reported below refer to this logarithmic quantity.

4.4 Earthquake networks

Baiesi and Paczuski [4] have applied the earthquake proximity η to analysis of earthquake graphs (a.k.a. networks). They considered a spanning graph whose vertices correspond, one-to-one, to the set of examined earthquakes. Each earthquake (vertex) j is connected to a single earlier (in time) earthquake i that minimizes the proximity η_{ij}. It is easy to check that this construction results in a time-oriented tree. The tree root corresponds to the first event in the catalog. Each event (except the first one) has a single parent (earlier event to which it is connected by an edge) and may have multiple offspring (later events to which it is connected by edges). It has been shown that the out-degree distribution in such graphs follows a power law decay with index $\gamma \approx -2$.

In this work, we consider a slightly different graph construction. Specifically, we construct graph $\mathcal{G}_{\eta_0}$ whose vertices correspond, one-to-one, to the observed earthquakes. The edges are formed between the pairs of vertices with proximity η below a threshold η_0. In general, a graph $\mathcal{G}_{\eta_0}$ is multi-component. Each connected component of $\mathcal{G}_{\eta_0}$ is a subgraph such that any pair of its vertices can be connected by a path that consists of edges each of which is shorter than η_0. Any two vertices from different connected components cannot be connected by such a path. In this work, we consider such earthquake graphs and measure the distance between two vertices either as the number of edges in the shortest path connecting them (unweighted, combinatorial graph), or as the minimal total edge lengths in such a path (weighted, metric graph).

4.5 δ-hyperbolicity with respect to the earthquake proximity η

In this study, we estimate δ-hyperbolicity with respect to the earthquake proximity η. We denote the respective hyperbolicity parameter as δ_η. We start by identifying transformations of time, space, and magnitude that have no effect on the resulting hyperbolicity.

Theorem 3 (Invariance of δ_η)**.** *Let us utilize the earthquake proximity formula* $\eta(x,y) = \log_{10}(t) + d\log_{10} r - bm_y, t_y \le t_x$*, where* $t = t_x - t_y$*,* r *is the Euclidean distance between the two points, and* d *is a constant. Then, a multiplicative transformation of space or time and an additive transformation of magnitude have no effect of the value of* δ_η*.*

Proof. First we consider a multiplicative transformation of the distance between points, r. Suppose $r' = C_r r$ for all r. Then

$$\begin{aligned}\eta'(x,y) &= \log_{10} t + d\log_{10} C_r r - bm_y \\ &= \log_{10} t + d\log_{10} r - bm_y + d\log_{10} C_r \\ &= \eta(x,y) + d\log_{10} C_r.\end{aligned} \tag{10}$$

Accordingly, we have for a quadruple $ABCD$:

$$\begin{aligned}\frac{L' - M'}{2} &= \frac{\eta'(A,B) + \eta'(C,D) - (\eta'(A,C) + \eta'(B,D))}{2} \\ &= \frac{\eta(A,B) + \eta(C,D) + 2d\log_{10} C_r - \eta(A,C) - \eta(B,D) - 2d\log_{10} C_r}{2} \\ &= \frac{L - M}{2}.\end{aligned} \tag{11}$$

Hence, a multiplicative transformation of the spatial variable r does not have an effect of the value of δ_η.

Next, we consider a multiplicative transformation of the time variable, $t' = C_t t$. Here we have

$$\begin{aligned}\eta'(x,y) &= \log_{10} C_t t + d\log_{10} r - bm_y \\ &= \log_{10} t + d\log_{10} r - bm_y + \log_{10} C_t \\ &= \eta(x,y) + \log_{10} C_t,\end{aligned} \tag{12}$$

and

$$\begin{aligned}\frac{L'-M'}{2} &= \frac{\eta'(A,B)+\eta'(C,D)-(\eta'(A,C)+\eta'(B,D))}{2} \\ &= \frac{\eta(A,B)+\eta(C,D)+2\log_{10} C_t-\eta(A,C)-\eta(B,D)-2\log_{10} C_t}{2} \\ &= \frac{L-M}{2}.\end{aligned} \tag{13}$$

Thus, a multiplicative transformation of the time variable, t, does not have an effect of the value of δ_η.

Finally, we consider an additive transformation of the magnitude variable, $m' = m + C_m$. Here

$$\begin{aligned}\eta'(x,y) &= \log_{10} t + d\log_{10} r - b(m_y + C_m) \\ &= \log_{10} t + d\log_{10} r - bm_y - bC_m \\ &= \eta(x,y) - bC_m,\end{aligned} \tag{14}$$

and

$$\begin{aligned}\frac{L'-M'}{2} &= \frac{\eta'(A,B)+\eta'(C,D)-(\eta'(A,C)+\eta'(B,D))}{2} \\ &= \frac{\eta(A,B)+\eta(C,D)-2bC_m-\eta(A,C)-\eta(B,D)+2bC_m}{2} \\ &= \frac{L-M}{2}.\end{aligned} \tag{15}$$

Thus, an additive transformation of the magnitude variable m, does not have an effect of the value of δ_η. This completes the proof. □

Theorem 3 ensures that the analysis of δ-hyperbolicity is independent of the units selected for time, distance, and energy measurements.

5. Hyperbolic property of earthquakes

We now focus on δ-hyperbolicity for seismicity. We use two complementary approaches – studying the space-time-magnitude domain of earthquakes using the earthquake proximity η, and earthquake proximity graphs using weighted and unweighted graph distances.

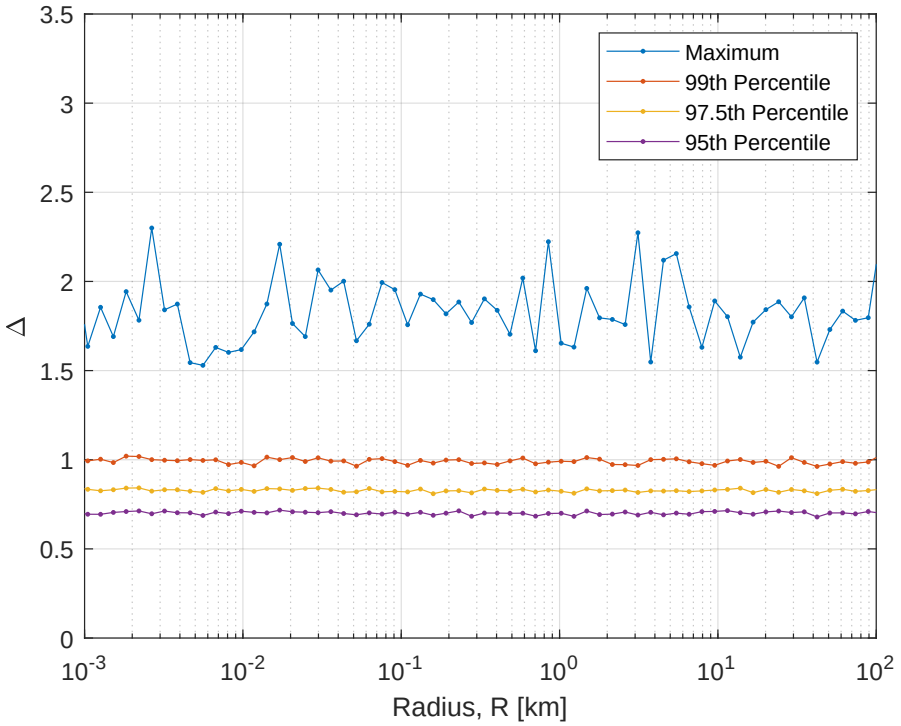

Figure 8: Δ vs R in a synthetic earthquake catalog. The experiment uses 10,000 uniform random quadruples for each value of R.

5.1 Synthetic catalogs

We start with analysis of synthetic catalogs, which allows us to generate quadruples, with a wide range of spatial, time, and magnitude components. Specifically, we work with a homogeneous Poisson model of seismicity. Every catalog is comprised of earthquakes that have uniform spatial coordinates in a circle of radius R, a uniform temporal coordinate on time interval $[0, T]$, and an exponential magnitude coordinate. The space, time, and magnitude components are independent. We use such synthetic catalogs to examine the dependence of $\Delta = (L - M)/2$ with respect to the range of each catalog component – space, time, and magnitude.

First, we inspect the relationship between Δ and the catalog radius R. We consider a range of radii to generate the spatial coordinates, and for each radius we generate the time coordinates uniformly on an interval $[0, T]$ with $T = 50$yrs, and the magnitude coordinates from an exponential distribution that is truncated by a maximal magnitude $m_{\max} = 6$. We create 10,000 quadruples for each radius and compute Δ for each quadruple, see Fig. 8. We see that Δ is independent of the spatial extent of the catalog.

Similarly, we look at the relationship between Δ and the time span of the catalog. We consider a range of durations T to generate the time coordinate on the interval $[0, T]$, and for each T we generate the spatial coordinates in a circle with constant radius $R = 100$km and the magnitude coordinates from an exponential distribution that is truncated by a maximal magnitude

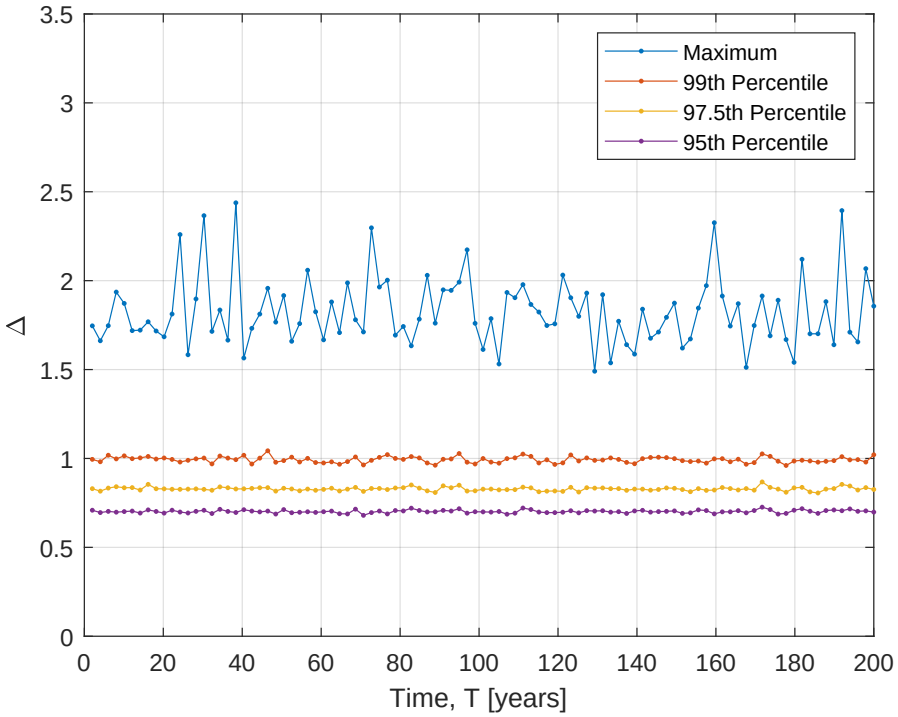

Figure 9: Δ vs T in a synthetic earthquake catalog. The experiment uses 10,000 uniform random quadruples for each value of T.

$m_{\max} = 6$. We create 10,000 quadruples for each upper time limit and compute Δ for each quadruple, see Fig. 9. We see that Δ is independent of the time span of the catalog.

Finally, we explore the relation between Δ and the magnitude range. We consider a range of upper magnitude truncation boundaries $m_{\max}$. For each $m_{\max}$, we generate the spatial coordinates in a circle with radius $R = 100$km and generate the time coordinates uniformly on an interval $[0, T]$ with $T = 50$ yrs. We generate 10,000 quadruples for each maximal magnitude value and compute Δ for each quadruple, see Fig. 10. We observe that Δ is only weakly dependent on $m_{\max}$, showing a slight increase for $m_{\max}$ within the interval $[1, 2]$. For larger values of $m_{\max} > 2$, the value of Δ again stabilizes.

In summary, our experiments (Figs. 8, 9, 10) suggest that $\Delta = (L - M)/2$ can take a range of values within the interval $[0, 2.5]$. The distribution of Δ is independent of spatial and time range of the examined earthquakes. The distribution depends weakly on the range of examined magnitudes, and remains bounded from above for the physically realistic magnitudes (recall that the largest recorded earthquake, that occurred in 1960 in Chile, had magnitude 9.5).

Next, we analyze the behavior of Δ in a synthetic catalog with respect to the diameter of the quadruple L. Recall (Fig. 3) that this behavior is closely related to the δ-hyperbolicity. We create 100,000 quadruples where each point has spatial coordinates generated uniformly in a circle with radius $R = 100$km, temporal coordinate generated uniformly on an interval $[0, T]$ with $T = 37$yrs (to match that in the catalog of Southern California), and magnitude coordinate

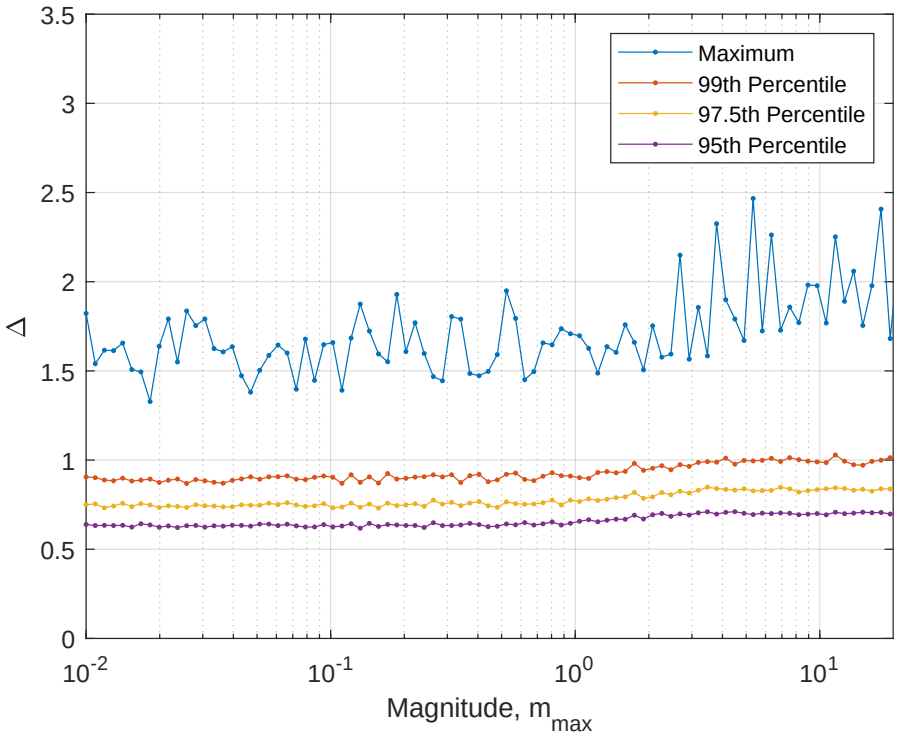

Figure 10: Δ vs $m_{\max}$ in a synthetic earthquake catalog. The experiment uses 10,000 uniform random quadruples for each value of $m_{\max}$.

generated exponentially and truncated by a range of maximal magnitudes $m_{\max}$. The range of maximal magnitudes is needed to produce a wide enough range of quadruple diameters. We then compute $\Delta = (L - M)/2$ for each quadruple. For each diameter L (up to some binning), we compute the maximum of Δ. The results are shown in Fig. 11. We see that the overall trend in both figures is similar to that of Fig. 3 in that Δ increases for smaller values of $L < 28$, and then stabilizes as L increases above $L = 28$. This hints at hyperbolic geometry of the earthquake space-time-magnitude domain with the earthquake proximity η. Notice that in the earthquake domain, we have to vary the maximal magnitude over almost two orders ($0.1 < m_{\max} < 7$) to obtain a wide range of quadruple diameters L. A fixed maximal magnitude always corresponds to a narrow range of L, insufficient to see the increase and stabilization of $\Delta = \Delta(L)$.

5.2 Real catalog

5.2.1 Earthquake proximity

We now examine the earthquake catalog of Southern California. We extract 10,000,000 quadruples from the catalog and for each quadruple compute the value of Δ and the corresponding diameter L. For each L, we compute the maximum and 99th, 97.5th, and 95th percentiles, see Fig. 12. As we know from the synthetic catalog experiments, a catalog with a fixed space, time, and magnitude range can only produce a limited range of quadruple diameters L. Accord-

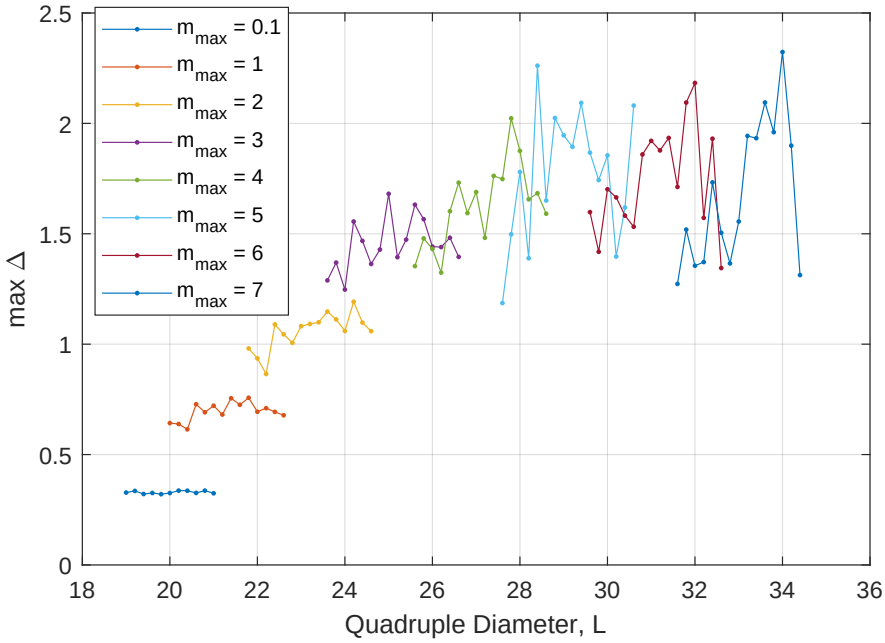

Figure 11: Maximum Δ vs L in a synthetic earthquake catalog. The experiment uses 100,000 uniform random quadruples for each value of $m_{\max}$; this results in 800,000 quadruples total.

ingly, we have to interpret the dependence $\Delta(L)$ with respect to this limited range. The range of quadruple diameters in this experiment is $38 < L < 45$. First, we observe that Δ slightly increases with L. This increase, however, is very different from what we observed in Euclidean space. The slope of a linear approximation to the empirical curve $\Delta(L)$ is significantly lower than 1, expected in a flat space. The observed value of Δ in all quadruples is below 3. Moreover, for the $\max \Delta(L)$, we see stabilization for larger L ($L > 42$). This behavior is reminiscent of the behavior of Δ in a hyperbolic space.

5.2.2 Combinatorial networks

We now shift our focus to δ-hyperbolicity in earthquake graphs. The graph is constructed by connecting the earthquakes (vertices) with proximity $\log_{10} \eta_{ij} < 15$. Then, we individually examine each connected subgraph with more than 500 vertices. From each selected subgraph, we select 10,000,000 random independent quadruples and compute the respective Δ and L.

We start with the combinatorial case, where the distance between vertices is measured as the number of edges in the minimal path between them. The results are shown in Fig. 13. Here, the range of observed quadruple diameters is $10 < L < 45$. The value of Δ is below 5.5 for all examined quadruples. Furthermore, $\Delta(L)$ increases with L within the interval $10 < L < 30$, and then stabilizes (end even slightly decreases for the largest quadruple diameters). The slope of the curve $\Delta(L)$ in the steepest part is not exceeding 0.1, which is smaller than the unit slope expected in a flat space.

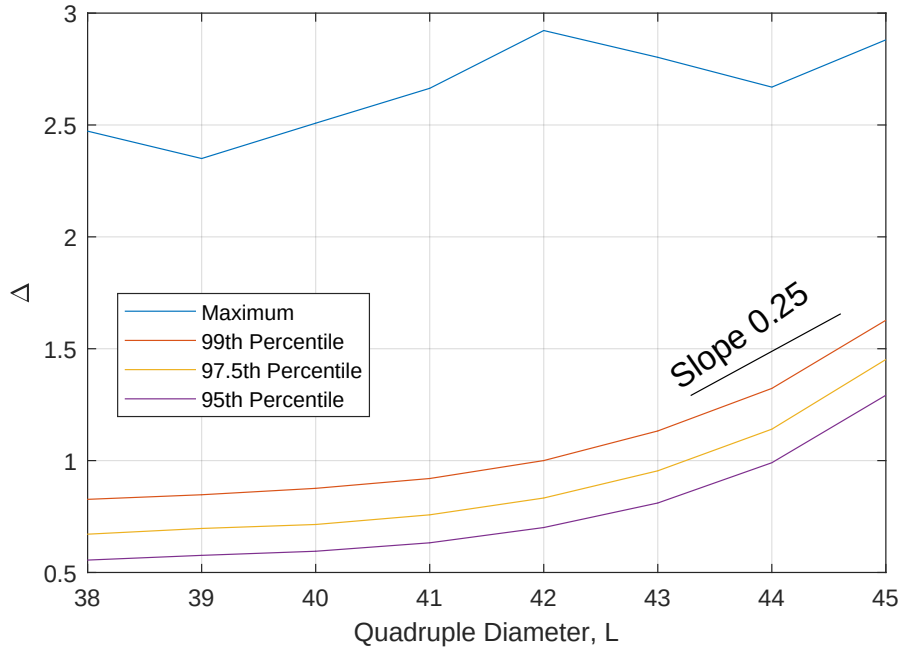

Figure 12: Δ vs L for real earthquake catalog of Southern California. The experiment uses 10,000,000 uniform random quadruples.

5.2.3 Metric networks

The results for metric graph, where the edge length equals the respective proximity, are shown in Fig. 14. Here, the range of quadruple diameters is $100 < L < 700$. The observed values of Δ are bounded from above by 80. The values of Δ increase with L within the interval $100 < L < 400$, and then stabilize (end even decrease for the largest diameters). The slope of the curve $\Delta(L)$ in the steepest part does not exceeds 0.2.

Overall, the qualitative behavior of $\Delta(L)$ in combinatorial and metric graphs is very similar and is reminiscent of that expected in a hyperbolic space. Accordingly, we conclude that the large-scale geometry of earthquake proximity graph is hyperbolic.

Figure 15 compares the actual earthquake proximity $\log_{10}\eta$ with that observed in combinatorial and metric graph for multiple pairs of earthquakes. This experiment uses the proximity threshold $\log_{10}\eta < 12$ and considers all connected subgraphs with at least 50 vertices. The clusters of (red) points in the plot correspond to the pairs of earthquakes separated by distinct numbers of edges in a metric graph (between 1 and 7). For events separated by a single edge, the actual proximity equal the graph separation; for other events, the actual proximity is smaller than the graph separation. The plot provides basic intuition behind the change of scale between Fig. 12 that refers to the actual earthquake proximity, and Figs. 13 and 14 that refer to unweighted and weighted graph analyses, respectively.

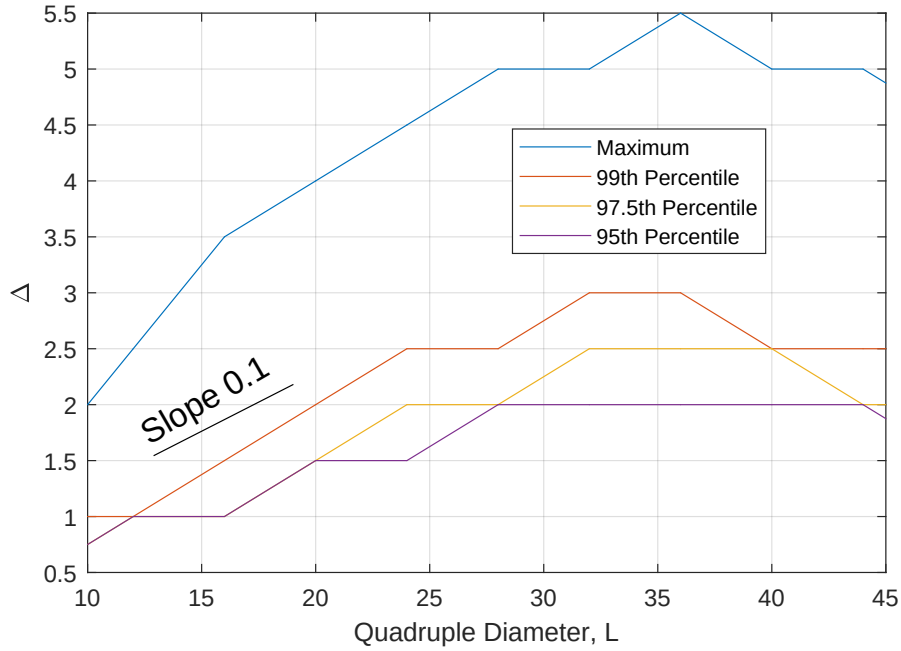

Figure 13: Δ vs L for unweighted (combinatorial) earthquake graph. The experiment uses 10,000,000 uniform random quadruples.

6. Discussion

This work examines the large scale geometric property of the space of observed earthquakes (Fig. 5,6) equipped with the Baiesi-Paczuski proximity (9). We estimate Gromov δ-hyperbolicity (Sect. 2.1) and find that in all conducted experiments the δ parameter is well bounded from above, and does not tend to increase with the linear dimension of the examined region. These properties characterize a hyperbolic metric space (Fig. 3) and suggest that a negatively curved hyperbolic geometry underlies the space-time-magnitude distribution of seismicity.

Our estimations are done in three complementary ways – in the time-space-magnitude domain D of earthquakes equipped with Baiesi-Paczuski proximity η (Fig. 12), in combinatorial proximity graphs (Fig. 13), and in metric proximity graphs (Fig. 14). That all estimations consistently suggest δ-hyperbolicity contributes to the robustness of our empirical results.

The stationary and homogeneous Poisson synthetic catalog also exhibit hyperbolic property (Sect. 5.1, Fig. 11). This suggests that the earthquake hyperbolicity is attributed to the general properties of the Baiesi-Paczuski earthquake proximity η rather than complex clustering and interactions of the observed earthquakes (see Fig. 6). At the same time, the values of quadruple diameter and Δ statistic reported in synthetic catalogs (Fig. 11) are slightly different from those for the observed earthquakes (Fig. 12). The effects of earthquake space-time clustering and other deviations from a homogeneous Poisson field on the hyperbolic property is an interesting problem that will be explored elsewhere.

The suggested hyperbolic geometry of earthquake field has the following immediate conse-

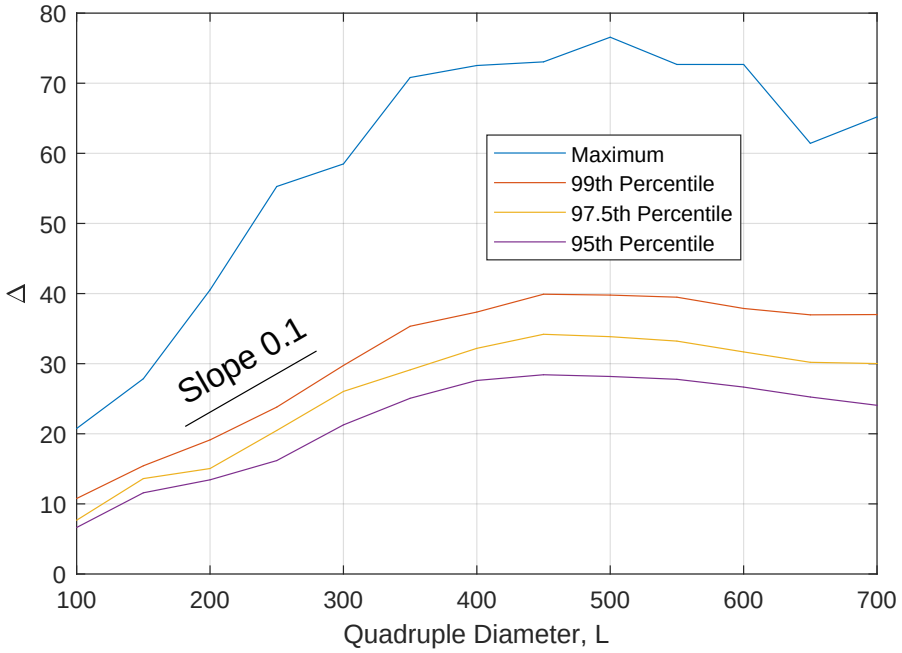

Figure 14: Δ vs L for weighted (metric) earthquake graph. The experiment uses 10,000,000 uniform random quadruples.

quences and interpretations:

(a) The complex heterogeneous space-time-energy characteristics of earthquakes are represented via a uniform distribution of points in a hyperbolic space. This interpretation needs to be further explored. It might be particularly useful for examining individual aftershock sequences and/or swarms.

(b) The power law degree distributions in earthquake networks [4] is explained via the results of *Krioukov et al.* [24].

(c) A useful insight is provided into the geometry of earthquake interactions [29] that can be interpreted and studied via hyperbolic geometry and curved space-time geodesics.

(d) The hyperbolic embedding suggests a natural neighborhood of an earthquake in space-time-energy domain. This domain can be used as a guide in analysis of aftershock/foreshock domains, and can facilitate aftershock/foreshock/swarm identification and earthquake declustering problem.

It remains an open problem to test the suggested hyperbolicity of the earthquake space using other models and data, and probably expand this framework to other phenomena and conceptual models related to seismicity. The latter include solar flare statistics, rock fracture (acoustic emission experiments), and a range of models explored within the self-organized criticality (SOC) framework.

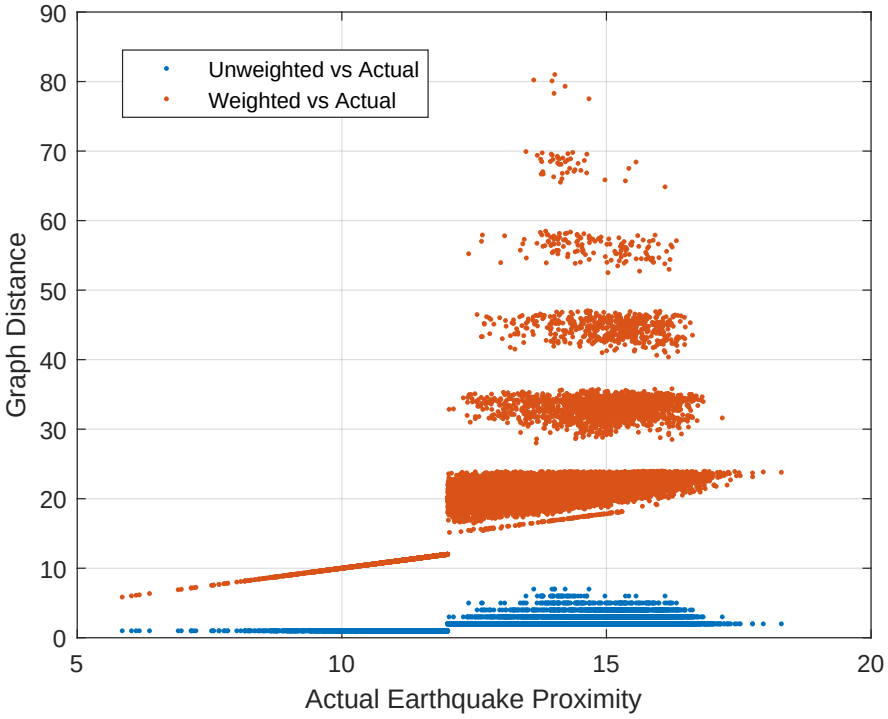

Figure 15: Comparison of actual earthquake proximity and graph distances, unweighted in blue and weighted in red.

A. Generating uniformly distributed points in hyperbolic circle

To generate uniformly distributed points in the hyperbolic circle, we use the following result.

Theorem 4 (Uniform point in hyperbolic circle)**.** *Suppose the point with polar coordinates* (r, θ) *is uniformly distributed in a hyperbolic circle of radius* R *centered at the origin. Then the probability density function of* r *is given by*

$$f(r) = \frac{\zeta \sinh \zeta r}{\cosh \zeta R - 1}, \quad 0 \leq r \leq R, \tag{16}$$

and the probability density functionof θ *is given by*

$$f(\theta) = \frac{1}{2\pi}, \quad 0 \leq \theta \leq 2\pi. \tag{17}$$

Proof. We observe that $\theta \sim \text{Uniform}[0, 2\pi)$ by circle symmetry. The distribution of the radius is found by examining the volume of hyperbolic space available at distance r from the origin. The area of a hyperbolic circle of radius r in a space of curvature $K = -\zeta^2$ is given by [6]:

$$A_\zeta(r) = \frac{2\pi}{\zeta^2}(\cosh \zeta r - 1). \tag{18}$$

Accordingly, the cumulative distribution function for the radius r is given by

$$F(r) = \frac{A_\zeta(r)}{A_\zeta(R)} = \frac{\frac{2\pi}{\zeta^2}\left(\cosh \zeta r - 1\right)}{\frac{2\pi}{\zeta^2}\left(\cosh \zeta R - 1\right)} = \frac{\cosh \zeta r - 1}{\cosh \zeta R - 1}. \tag{19}$$

We differentiate to get the probability density function:

$$f(r) = F'(r) = \frac{\zeta \sinh \zeta r}{\cosh \zeta R - 1}. \tag{20}$$

This completes the proof. □

To simulate a uniform point in a hyperbolic circle, we use a uniform random variable $u \sim \mathrm{Uniform}[0, 1]$ and apply the inverse transform:

$$u = \frac{\cosh \zeta r - 1}{\cosh \zeta R - 1}. \tag{21}$$

Solving for r, we get

$$u\left(\cosh \zeta R - 1\right) = \cosh \zeta r - 1, \tag{22}$$

which finally gives

$$r = F^{-1}(u) = \frac{\mathrm{acosh}((u\left(\cosh \zeta R - 1\right) + 1))}{\zeta}. \tag{23}$$

References

[1] Abe, S., & Suzuki, N. (2004) Scale-free network of earthquakes. *Europhysics Letters,* 65(4), 581.

[2] Abe, S., & Suzuki, N. (2006) Complex-network description of seismicity. *Nonlinear Processes in Geophysics*, 13(2), 145–150.

[3] Abu-Ata, M., & Dragan, F. F. (2016) Metric tree-like structures in real-world networks: an empirical study. *Networks*, 67(1), 49–68.

[4] Baiesi, M., & Paczuski, M. (2004) Scale-free networks of earthquakes and aftershocks. *Physical Review E*, 69(6), 066106.

[5] Ben-Zion, Y. (2008) Collective behavior of earthquakes and faults: Continuum-discrete transitions, progressive evolutionary changes, and different dynamic regimes. *Reviews of Geophysics*, 46(4).

[6] Bonahon, F. (2009) Low-dimensional geometry: From Euclidean surfaces to hyperbolic knots (Vol. 49). *American Mathematical Soc.*

[7] Borassi, M., Chessa, A., & Caldarelli, G. (2015) Hyperbolicity measures democracy in real-world networks. *Physical Review E*, 92(3), 032812.

[8] Bridson, M. R., & Haefliger, A. (2013) *Metric spaces of non-positive curvature* (Vol. 319). Springer Science & Business Media.

[9] Burago, D., Burago, I. D., Burago Y., Ivanov, S. A., & Ivanov, S. (2001) A course in metric geometry (Vol. 33). *American Mathematical Soc.*.

[10] Cannon, J. W., Floyd, W. J., Kenyon, R., & Parry, W. R. (1997) Hyperbolic geometry. *Flavors of geometry*, 31, 59–115.

[11] Chen, W., Fang, W., Hu, G., & Mahoney, M. W. (2013) On the hyperbolicity of small-world and treelike random graphs. *Internet Mathematics*, 9(4), 434–491.

[12] Cohen, N., Coudert, D., & Lancin, A. (2012) Exact and approximate algorithms for computingthe hyperbolicity of large-scale graphs. [Research Report] RR-8074, INRIA. `hal-00735481v4`

[13] Davidsen, J., & Baiesi, M. (2016) Self-similar aftershock rates. *Physical Review E*, 94(2), 022314.

[14] Davidsen, J., Grassberger, P., & Paczuski, M. (2006) Earthquake recurrence as a record breaking process. *Geophysical Research Letters*, 33(11).

[15] Davidsen, J., Kwiatek, G., Charalampidou, E. M., Goebel, T., Stanchits, S., Rück, M., & Dresen, G. (2017) Triggering processes in rock fracture. *Physical review letters*, 119(6), 068501.

[16] Ellsworth, W. L. (2013) Injection-induced earthquakes. *Science*, 341(6142), 1225942.

[17] Fournier, H., Ismail, A., & Vigneron, A. (2015) Computing the Gromov hyperbolicity of a discrete metric space. *Information Processing Letters*, 115(6–8), 576–579.

[18] Gentili, S., Di Giovambattista, R., & Peresan, A. (2017) Seismic quiescence preceding the 2016 central Italy earthquakes. *Physics of the Earth and Planetary Interiors*, 272, 27–33.

[19] Gu, C., Schumann, A. Y., Baiesi, M., & Davidsen, J. (2013) Triggering cascades and statistical properties of aftershocks. *Journal of Geophysical Research: Solid Earth*, 118(8), 4278–4295.

[20] Hauksson, E., Yang, W., & Shearer, P. M. (2012) Waveform relocated earthquake catalog for southern California (1981 to June 2011). *Bulletin of the Seismological Society of America*, 102(5), 2239–2244.

[21] Jonckheere, E., Lohsoonthorn, P., & Ariaei, F. (2011) Scaled Gromov four-point condition for network graph curvature computation. *Internet Mathematics*, 7(3), 137–177.

[22] Kennedy, W. S., Narayan, O., & Saniee, I. (2013) On the hyperbolicity of large-scacle networks. *Preprint* arXiv:1307.0031.

[23] Krioukov, D., Papadopoulos, F., Vahdat, A., & Boguná, M. (2009) Curvature and temperature of complex networks. *Physical Review E*, 80(3), 035101.

[24] Krioukov, D., Papdopoulos, F., Kitsak, M., Vahdat, A., & Bogunaá, M. (2010) Hyperbolic geometry of complex networks. *Physical Review E*, 82(3), 036106

[25] Nica, B., & Spakula, J. (2014) Strong hyperbolicity. *Preprint* arXiv:1408.0250.

[26] Nowak, P. W., & Yu, G. (2012) *Large scale geometry.* EMS Textbooks in Mathematics, European Mathematical Society, urldoi:10.4171/112

[27] Phillips, J. D., Schwanghart, W., & Heckmann, T. (2015) Graph theory in the geosciences. *Earth-Science Reviews*, 143, 147–160.

[28] Schoenball, M., Davatzes, N. C., & Glen, J. M. (2015). Differentiating induced and natural seismicity using space-time-magnitude statistics applied to the Coso Geothermal field. *Geophysical Research Letters*, 42(15), 6221–6228.

[29] Stein, R. S. (2003) Earthquake conversations. *Scientific American*, 288(1), 72–79.

[30] Telesca, L., & Lovallo, M. (2012) Analysis of seismic sequences by using the method of visibility graph. *Europhysics Letters*, 97(5), 50002.

[31] Tenenbaum, J. N., Havlin, S., & Stanley, H. E. (2012) Earthquake networks based on similar activity patterns. *Physical Review E*, 86(4), 046107.

[32] Weinberger, S. (2015) Book review of *Large scale geometry* by P.Nowak and G.Yu *Bulletin of American Mathematical Society,* 52(1), 141–149.

[33] Zaliapin, I., Gabrielov, A., Keilis-Borok, V., & Wong, H. (2008) Clustering analysis of seismicity and aftershock identification. *Physical Review Letters*, 101(1), 018501.

[34] Zaliapin, I., & Ben-Zion, Y. (2013) Earthquake clusters in southern California I: Identification and stability. *Journal of Geophysical Research: Solid Earth*, 118(6), 2847–2864.

[35] Zaliapin, I., & Ben-Zion, Y. (2013) Earthquake clusters in southern California II: Classification and relation to physical properties of the crust. *Journal of Geophysical Research: Solid Earth*, 118(6), 2865–2877.

[36] Zaliapin, I., & Ben-Zion, Y. (2016) Discriminating characteristics of tectonic and human-induced seismicity. *Bulletin of the Seismological Society of America*, 106(3), 846–859.

[37] Zaliapin, I., & Ben-Zion, Y. (2016) A global classification and characterization of earthquake clusters. *Geophysical Journal International*, 207(1), 608–634.